

The Genetic Architecture of Biological Age in Nine Human Organ Systems

Short title: Genetics of Multi-Organ Biological Age Gap

One-sentence summaries: Across nine human organ systems, the genetic architectures of the biological age gap (BAG) revealed BAG-organ specificity and inter-organ crosstalk, highlighting the interconnections among multiple organ systems, chronic diseases, body weight, and lifestyle factors.

Junhao Wen^{1,2,3*}, Ye Ella Tian⁴, Ioanna Skampardoni², Zhijian Yang², Elizabeth Mamourian², Filippos Anagnostakis⁵, Bingxin Zhao⁶, Arthur W. Toga³, Andrew Zalesky⁴, Christos Davatzikos²

¹Laboratory of AI and Biomedical Science (LABS), Stevens Neuroimaging and Informatics Institute, Keck School of Medicine of USC, University of Southern California, Los Angeles, California, USA

²Artificial Intelligence in Biomedical Imaging Laboratory (AIBIL), Center for AI and Data Science for Integrated Diagnostics (AI²D), Perelman School of Medicine, University of Pennsylvania, Philadelphia, USA

³Laboratory of Neuro Imaging (LONI), Stevens Neuroimaging and Informatics Institute, Keck School of Medicine of USC, University of Southern California, Los Angeles, California, USA

⁴Melbourne Neuropsychiatry Centre, Department of Psychiatry, Melbourne Medical School, The University of Melbourne, Melbourne, Victoria, Australia

⁵Department of Medical and Surgical Sciences, University of Bologna, 40126 Bologna, Italy

⁶Department of Statistics and Data Science, University of Pennsylvania, Philadelphia, PA, USA

*Corresponding author:

Junhao Wen, junhao.wen@usc.edu

2025 Zonal Ave, Los Angeles, CA 90033, United States

Word counts: 5701 words

Abstract

Understanding the genetic basis of biological aging in multi-organ systems is vital for elucidating age-related disease mechanisms and identifying therapeutic interventions. This study characterized the genetic architecture of the biological age gap (BAG) across nine human organ systems in 377,028 individuals of European ancestry from the UK Biobank. We discovered 393 genomic loci, including 143 novel loci, associated with the BAG of the brain, eye, cardiovascular, hepatic, immune, metabolic, musculoskeletal, pulmonary, and renal systems. We also observed BAG-organ specificity and inter-organ crosstalk. Genetic variants associated with the nine BAGs are predominantly specific to the respective organ system while exerting pleiotropic effects on traits linked to multiple organ systems. A gene-drug-disease network confirmed the involvement of the metabolic BAG-associated genes in drugs targeting various metabolic disorders. Genetic correlation analyses supported Cheverud's Conjecture¹ – the genetic correlation between BAGs mirrors their phenotypic correlation. A causal network revealed potential causal effects linking chronic diseases (e.g., Alzheimer's disease), body weight, and sleep duration to the BAG of multiple organ systems. Our findings shed light on promising therapeutic interventions to enhance human organ health within a complex multi-organ network, including lifestyle modifications and potential drug repositioning strategies for treating chronic diseases. All results are publicly available at: <https://labs.loni.usc.edu/medicine>.

Main

Biological aging is complex and influenced by many factors, including genetics², environmental exposures³, and modifiable lifestyle factors⁴ across multiple organ systems. A comprehensive understanding of the phenotypic landscape and genetic architecture underlying biological aging in multiple human organ systems is paramount in forging the path toward precision medicine⁵, including identifying vulnerability (e.g., smoking) and resilience factors (e.g., physical activities). This knowledge can improve our understanding of the underlying mechanisms driving age-related diseases, identify novel therapeutic targets, and develop personalized interventions for maintaining health and functional independence in the aging population.

Previous research efforts have made progress in studying the interconnectedness of multi-organ systems in human health^{3,6–13}. In a recent study by McCracken et al., a heart-brain-liver axis was studied, highlighting direct and indirect associations among the three organs and their interconnectivity and shared biological pathways¹¹. A recent review highlighted the role of inter-organ signals in metabolic control, including the secretion of peptides, small molecules, and lipid mediators by metabolic tissues and the involvement of the central nervous system in coordinating peripheral metabolic functions⁹. Riding the crest of the wave of artificial intelligence (AI), the biomedical community has increasingly adopted the biological age gap (BAG) as a comprehensive biomarker of human aging in multiple human organ systems. Specifically, BAG serves as a quantitative phenotype to capture the disparity between an individual's AI-derived age and chronological age, which can be used to model aging-related normative trajectory at the individual level and holds potential for application in disease populations to capture pertinent pathological processes. Nie et al. first derived the biological age in nine organ systems to predict the possibility of becoming centenarian¹³. In another study, Tian et al. derived eight BAGs in eight organ systems, correlating them with cognition, chronic disease, lifestyle factors, and mortality³.

However, genetic determinants and biological pathways that underlie the observed heterogeneity of organ-specific BAGs remain elusive. Furthermore, whether chronic diseases and lifestyle factors causally impact the divergence between predicted age and chronological age in these organ systems remains to be established, manifesting as either a younger or older biological age. Our previous genome-wide association study (GWAS) uncovered the genetic heterogeneity of the multimodal brain BAGs using magnetic resonance imaging (MRI) data¹⁴. Expanding on prior research, the current study sought to comprehensively depict the genetic architecture underlying biological aging across nine human organ systems, including the brain, cardiovascular, eye, hepatic, immune, metabolic, musculoskeletal, pulmonary, and renal BAGs. Our overarching hypothesis postulates that the genetic determinants associated with the nine BAGs are not only specific to individual organ systems (i.e., BAG-organ specificity) but also directly or indirectly interconnected with other organ systems (i.e., inter-organ crosstalk).

In the current study, we analyzed multimodal data from 377,028 individuals of European ancestry in the UK Biobank study¹⁵ (UKBB) to comprehensively capture the genetic architecture of the nine organ systems (**Method 1**). First, we used data from 154,774 participants to perform GWAS, gene-level, partitioned heritability, and genetic correlation analyses (**Method 2**). In our Mendelian randomization analyses, we used 222,254 UKBB participants that did not overlap with the individuals used to compute BAG to avoid potential bias¹⁶. We *i*) identified both previously reported and novel genomic loci, *ii*) demonstrated a greater genetic heritability estimate for the brain BAG compared to other organ systems, *iii*) constructed a network linking genes, drugs, and diseases for potential drug repurposing, *iv*) confirmed that BAG-associated

variants and genes exhibit BAG-organ specificity and inter-organ crosstalk, and v) established both genetic correlations and causal networks among the nine BAGs, chronic diseases, and lifestyle factors. All results, including the GWAS summary statistics, are publicly accessible through the MEDICINE (Multi-organ biomEDical sCIeNcE) knowledge portal: <https://labs.loni.usc.edu/medicine>.

Results

Genome-wide associations identify 143 novel genomic loci associated with the nine

biological age gaps

GWAS (**Method 2a**) identified 11, 44, 17, 41, 61, 76, 24, 67, and 52 genomic loci significantly associated with the brain, cardiovascular, eye, hepatic, immune, metabolic, musculoskeletal, pulmonary, and renal BAGs, respectively (**Fig. 1**, and **Supplementary eFile 1**). Notably, 143 loci are novel – their top lead single-nucleotide polymorphism (SNP) was never associated with any clinical traits in the EMBL-EBI GWAS Catalog¹⁷, as annotated by the top lead SNPs in **Fig. 1 (Method 2c)**. Specifically, 7, 18, 7, 11, 27, 14, 11, 26, and 22 novel loci were found for the abovementioned nine BAGs.

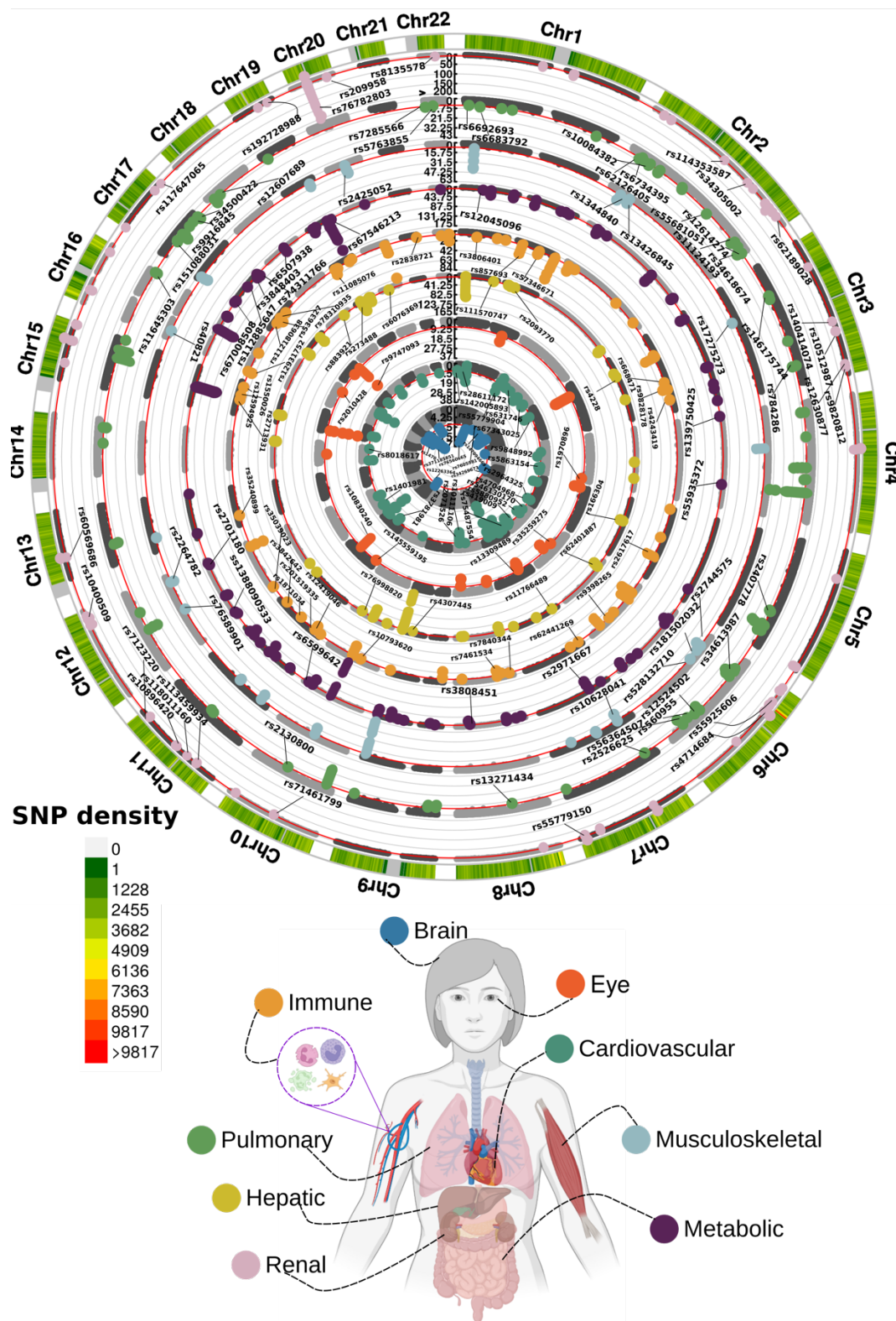
Some genomic loci were distinctly associated with a specific organ, while others showed associations with multiple organ BAGs or were close to each other on the genome. For instance, the locus on chromosome 6 associated with the hepatic (rs62401887, position: 24416482 at 6p22.3), immune (rs80215559, position: 25918225 at 6p22.3), metabolic (rs79220007, position: 26098474 at 6p22.2), musculoskeletal (rs2744575, position: 24494975 at 6p22.3), pulmonary (rs411535, position: 22061040 at 6p22.3), and renal BAGs (rs55925606, position: 25878848 at 6p22.2) was close with each other on the human genome. Bayesian colocalization¹⁸ analyses supported a causal association of SNPs within this locus with the liver and musculoskeletal BAGs. The results showed a posterior possibility (PP) of two distinct causal variants (PP.H3.ABF=0.744) or one shared causal variant (PP.H4.ABF=0.256) associated with both traits in the *GPLD1* gene, although the PP.H4.ABF hypothesis did not achieve the suggested threshold (>0.8)¹⁸. Detailed results are presented in **Supplementary eFigure 1**.

Many of these loci were mapped to protein-encoding genes and provided functional insights. For example, the top lead SNP (rs62401887 at 6p22.3) within the locus of the hepatic BAG was mapped to the *MRS2* gene by position (with a deleterious score of 14.89) and expression quantitative trait loci (eQTL, P-value=1.09x10⁻¹⁰) (**Method 2c**), which enables magnesium ion transmembrane transporter activity. We illustrate the regional Manhattan plot for the genomic locus with the highest significance for each organ BAG in **Supplementary eFigure 2**. For instance, the brain BAG exhibited a highly significant locus (top lead SNP: rs371185851 at 17q21.31) with multiple protein-encoding genes, including the widely recognized *MAPT* gene encoding tau protein associated with neurodegenerative diseases, such as Alzheimer's disease (AD)¹⁹. Moreover, the SNPs within this locus included enhancers and transcription start sites, specific to brain tissue chromatin states, highlighting their functional relevance in brain-related processes (**Supplementary eFigure 2a**).

Consistent results were observed in split-sample and sex-stratified analyses (**Method 2a** and **Supplementary eFigures 3-13**). In the GWAS from the first split, we found 143, 399, 145, 1358, 571, 1731, 527, 1232, and 1194 BAG-SNP associations for the nine abovementioned BAGs (P-value < 5x10⁻⁸). Of these, 67 (51), 375 (316), 143 (137), 1338 (1209), 563 (448), 1725 (1339), 527 (496), 1232 (762), and 1183 (1093) associations were replicated in the second split

using both the nominal P-value (<0.05 , 82% replications) and the Bonferroni-corrected threshold ($<0.05/N$, 80% replications). For the female-specific GWAS, we observed 352, 269, 398, 3524, 1462, 1726, 1759, 536, and 1334 BAG-SNP associations for the nine BAGs. Among these, 349 (346), 210 (140), 253 (206), 1648 (488), 1171 (840), 1461 (1095), 495 (108), 529 (375), and 1247 (1089) associations were replicated in the male-specific GWAS using both the nominal P-value (<0.05 , 65% replications) and the Bonferroni-corrected threshold ($<0.05/N$, 41% replications). While we observe fewer significant loci ($P\text{-value} < 5 \times 10^{-8}$) in the sensitivity analyses than the results obtained from the full sample sizes, which may be due to reduced sample sizes, the signal peaks of the P-values remain consistent (**Supplementary eFigure 5-13**), as well as the effect directions. Sex differences were most evident in the musculoskeletal BAG. Only one genomic locus (at 2p23.3) was associated with both females and males for the musculoskeletal BAG (**Supplementary eFigure 4 and 11**). Detailed results of these loci are presented in **Supplementary eFile 2** for split-sample and **Supplementary eFile 3** for sex-stratified results, respectively.

Figure 1: 143 novel genomic loci of the nine biological age gaps



Organ-specific biological age gap (BAG) was derived from a large cohort of 30,108 to 111,543 European ancestry participants from the UK Biobank cohort. The nine organ systems include the

brain ($N=30,108$), cardiovascular ($N=111,543$), eye ($N=36,004$), hepatic ($N=111,543$), immune ($N=111,543$), metabolic ($N=111,543$), musculoskeletal ($N=111,543$), pulmonary ($N=111,543$), and renal ($N=111,543$) BAGs. 143 novel genomic loci were associated with the nine BAGs using a genome-wide P-value threshold [$-\log_{10}(\text{P-value}) > 7.30$]. For visualization purposes, we only denoted the novel genomic loci – not associated with any clinical traits in EMBL-EBI GWAS Catalog – using their top lead SNP. The anatomical illustration of the human body was created using [BioRender.com](https://www.biorender.com). All analyses used the Genome Reference Consortium Human Build 37 (GRCh37).

Phenome-wide associations demonstrate organ system specificity and inter-organ crosstalk

We aimed to investigate the agreement of the identified genomic loci through our analysis of existing GWAS literature. To this end, we performed a phenome-wide association query in the EMBL-EBI GWAS Catalog¹⁷ for the candidate and independent significant SNPs within each locus (**Method 2d**).

Our findings demonstrated significant associations between the identified loci in our GWAS and clinical traits in the literature specific to each organ system (i.e., BAG-organ specificity) (**Fig. 2a**). The genomic loci associated with the brain BAG exhibited the highest proportion of associations (529 out of 1798) with traits related to the brain, including imaging-derived phenotypes such as brain volume metrics and white matter microstructure, demonstrated in the keyword cloud presented in **Fig. 2a**. The brain BAG loci were also enriched in many other traits related to other organ systems and chronic diseases, evidencing inter-organ crosstalk, including metabolic ($N=383/1798$, e.g., cholesterol levels), musculoskeletal ($N=84$, e.g., height), lifestyle factors ($N=115/1798$, e.g., alcohol consumption), neurodegenerative traits ($N=210/1798$, e.g., AD), and cognition ($N=79/1798$). For the eye BAG loci, most associations were found in metabolic (203 out of 1053), musculoskeletal ($N=186/1053$), eye ($N=144/1053$, e.g., age-related macular degeneration), and brain traits ($N=47/1053$), among many others.

For the other seven body organ systems, among the loci associated with the cardiovascular BAG, most associations were observed with cardiovascular traits (1296 out of 1890), such as systolic/diastolic blood pressure and coronary artery disease. Other associations were found with musculoskeletal ($N=154/1890$), metabolic ($N=130/1890$), immune ($N=54/1890$), renal ($N=48/1890$), and brain ($N=39/1890$) traits. For the hepatic BAG loci, 3769 out of 7216 associations were related to metabolic and 1127 hepatic traits (e.g., blood protein, cirrhosis, and bilirubin). Among the loci associated with the immune BAG, abundant associations were found in metabolic (2028 out of 4453), immune ($N=884/4453$, e.g., different types of immune cells), hepatic ($N=319/4453$), musculoskeletal ($N=243/4453$), and cardiovascular traits ($N=190/4453$). For the metabolic BAG loci, most associations were observed in metabolic traits (22417 out of 26780). We found a significant intertwining of metabolic systems with other organ systems, highlighting the presence of inter-organ crosstalk in human metabolic activities. This was supported by the fact that metabolic traits were highly enriched in the musculoskeletal (1301 out of 2869), pulmonary (305 out of 4547), and renal (2206 out of 4839) BAGs. Details of the phenome-wide associations are presented in **Supplementary eFile 4**.

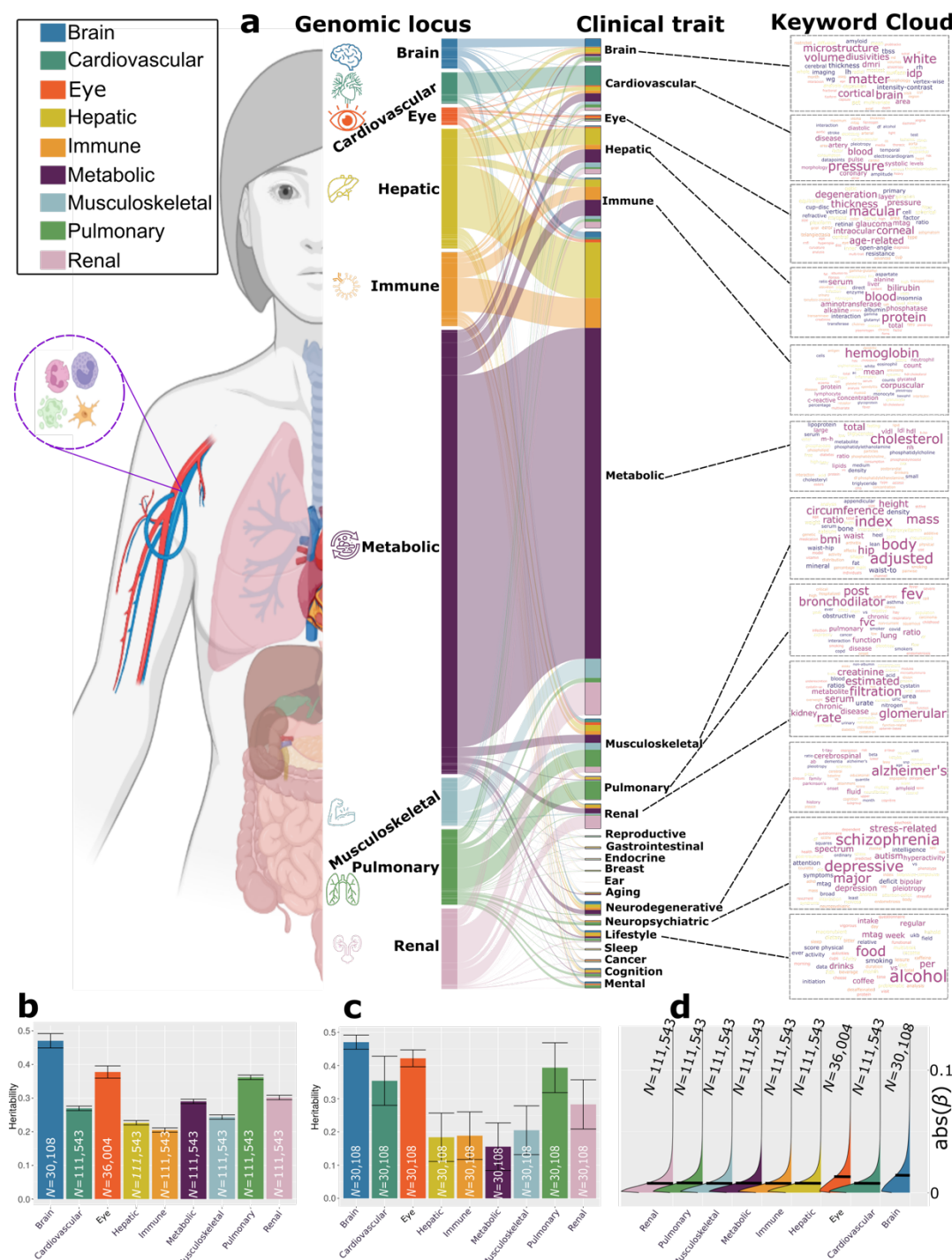
The biological age gap is more heritable in the brain than in other organ systems

To enable a fair comparison of organ age heritability (i.e., effect size), we estimated the SNP-based heritability (h^2) across the nine organ systems using both the full sample sizes (**Fig. 2b**)

and down-sampled comparable samples (**Fig. 2c**). Additionally, the distributions of the magnitude of the beta coefficient (β) in GWAS are shown in Fig. **2d**.

Upon analyzing the full sample sizes, the estimated h^2 for the brain BAG (0.47 ± 0.02) significantly outperformed all other organ systems, followed by the eye (0.38 ± 0.02), pulmonary (0.36 ± 0.006), renal (0.31 ± 0.006), metabolic (0.29 ± 0.006), cardiovascular (0.27 ± 0.006), musculoskeletal (0.24 ± 0.006), hepatic (0.23 ± 0.006), and immune BAGs (0.21 ± 0.006) (**Fig. 2b**). All heritability estimates were statistically significant after controlling for multiple comparisons using the Bonferroni correction. This trend persisted even when subsampling the population of other BAGs to match that of the brain BAG, with comparable distributions in sex and age (**Fig. 2c**). Finally, the effect size in the GWAS of the brain BAG ($\beta = 0.014 \pm 0.015$) was also larger than other organ systems: $0.007 < \beta < 0.008$ for the seven body organ BAGs and $\beta = 0.013 \pm 0.014$ for the eye BAG (**Fig. 2d**). Detailed results of the h^2 estimate are presented in **Supplementary eTable 1**.

Figure 2: Phenome-wide associations of the identified genomic loci and SNP-wide heritability estimates of the nine biological age gap



a) Phenome-wide associations of the identified genomic loci in the EMBL-EBI GWAS Catalog. By examining the candidate and the independent significant SNPs within each genomic locus, we linked them to various clinical traits through a comprehensive query. These traits were categorized into high-level groups encompassing different organ systems, neurodegenerative and

neuropsychiatric disorders, and lifestyle factors. To visually represent the findings, we generated keyword cloud plots based on the frequency of these clinical traits within each BAG. The length of each rectangle block indicates the number of associations concerning the genomic loci in our analysis and clinical traits in the literature. **b)** SNP-based heritability estimates (h^2) for the nine BAGs with full sample sizes. **c)** The estimated h^2 using randomly down-sampled sample sizes ($N=30,108$) for the nine BAGs. Error bars represent the standard error of the estimated parameters. **d)** The kernel density estimate plot shows the distribution of the effect sizes (i.e., the magnitude of the linear regression β coefficients) in the nine GWAS. The black horizontal lines represent the mean effect sizes.

Genes linked to the nine biological age gaps are implicated in organ system-specific biological pathways

To biologically validate our GWAS findings at the gene level, we performed gene-based associations using the MAGMA²⁰ software based on the full P-value distribution from the GWAS of the nine BAGs. The significantly associated genes (**Supplementary eFile 5**) were used for the gene set enrichment analysis (GESA, **Method 2e**) to annotate relevant biological pathways underlying each organ system (**Fig. 3a**).

Genes associated with the cardiovascular BAG were implicated in the insulin-like growth factor II binding (IGF-II) pathway (P-value= 7.08×10^{-7}). Genes associated with the eye BAG were enriched in the pathway of forebrain dorsal-ventral pattern (FDVP) formation (P-value= 6.46×10^{-7}). Among others, the most significant enrichment result shown in the hepatic BAG was the flavonoid glucuronidation pathway (P-value= 1.71×10^{-8}). Genes linked to the metabolic BAG displayed enrichment in several pathways, including the flavonoid glucuronidation pathway (P-value= 2.46×10^{-15}) and triglyceride-rich lipoprotein particle clearance pathway (P-value= 3.72×10^{-15}), both of which are implicated in liver function. In addition, the neutral lipid metabolic process, regulated by complex pathways featuring lipid metabolism enzymes and structural proteins, was also identified. Genes associated with the musculoskeletal BAG exhibited enrichment in the gene set in an amplicon at 20q11 (P-value= 1.54×10^{-15}), defined by a study of copy number alterations conducted on 191 patients with breast tumors²¹. Genes associated with the pulmonary BAG displayed significant enrichment in the pathways of the negative regulation biosynthetic process (P-value= 3.72×10^{-10}), consistent with a previous DNA methylation analysis of pulmonary function using old-aged Chinese monozygotic twins²². Genes associated with the renal BAG were implicated in the xenobiotic glucuronidation pathway (P-value= 1.56×10^{-6}). Given that the kidney contains most enzymes metabolizing foreign substances (i.e., xenobiotics), it plays a crucial role in the overall metabolism of drugs and other foreign compounds within the body (**Fig. 3a**). Detailed results of GESA are presented in **Supplementary eFile 6**.

Genes linked to the nine biological age gaps display organ system-specific gene expression patterns

To investigate the gene expression patterns of the significant genes associated with the nine BAGs, we performed a tissue-specific gene expression analysis²⁰ using MAGMA and the GTEx RNA-seq dataset²³ (**Method 2f**).

Across 54 human organ tissues (**Fig. 3b**), genes associated with the cardiovascular BAG exhibited significant overexpression in various heart-related tissues (e.g., the aorta and tibial artery) and other organs (e.g., the uterus and colon sigmoid). Genes associated with the hepatic BAG were overexpressed in the liver and adipose subcutaneous. Several immune system-related tissues showed a high average expression of the genes related to the immune BAG, including the spleen, blood, and lymphocytes. Likewise, the genes associated with the metabolic BAG showed a high expression level in the liver and intestine – critical organs in the metabolic system. The genes related to the pulmonary BAG displayed significant overexpression in the esophagus gastroesophageal junction, artery, and others. The genes associated with the renal BAG were overexpressed in the kidney. Detailed results are presented in **Supplementary eFile 7**.

Gene-drug-disease network substantiates potentially repositionable drugs for aging-related diseases

We performed a drug target enrichment analysis²⁴ for the genes linked to the nine BAGs in the targeted gene sets of drug categories using the DrugBank database²⁵, thereby constructing a gene-drug-disease network of potentially repositionable drugs (**Method 2g**).

The constructed gene-drug-disease network (**Fig. 3c**) identified significant interactions between 12 metabolic BAG-linked genes, 46 drugs, and many metabolic disorders encoded in the ICD10 code (E70-E90). For instance, the *PPARD* gene was the target gene of the PPAR- δ agonist (SAR 351034, denoted in **Fig. 3c**), which aimed to improve insulin sensitivity and lipid-related activities and battle against inflammation and oxidative stress, serving as actionable drugs for metabolic disorders, diabetes, and kidney and liver injury-related diseases²⁶. Our results showed that genes associated with the metabolic BAG were used to develop drugs treating various other diseases – beyond metabolic disorders – related to multiple organ systems (**Fig. 3c**). These included heart-related diseases (e.g., chronic rheumatic heart diseases for I05-I09) and cerebrovascular disease (I60-I69), although the enrichment did not survive correction for multiple comparisons (**Fig. 3c**). For instance, the drug MPSK3169A (clinical trial number: NCT01609140; metabolic BAG linked gene: *PCSK9*) is used to treat cerebrovascular disease and coronary heart disease; T3D-959 (clinical trial number: NCT04251182; pulmonary BAG linked gene: *PPARD*), was a candidate drug targeting AD. Detailed results are presented in **Supplementary eFile 8**.

The drug-gene-disease network reveals the association between genes related to the metabolic BAG and drugs targeting various chronic diseases. It highlights the importance of the metabolic system in the overall functioning of the human body and the potentials of repositioning existing drugs to tackle biological aging.

Bonferroni correction. Abbreviation: ICD: International Classification of Diseases; EGJ: esophagus gastroesophageal junction.

Heritability enrichment in different cell types, functional categories, tissue-specific gene expression, and chromatin states

To further biologically validate our GWAS findings at the SNP level, we performed partitioned heritability analyses²⁷ (**Method 2i**) to estimate the heritability enrichment of genetic variants related to the nine BAGs concerning three different cell types²⁸ (i.e., neurons, oligodendrocytes, and astrocytes, **Fig. 4a**), 53 non-tissue-specific functional categories²⁷ (**Fig. 4b**), 205 tissue-specific gene expression data²³ (**Fig. 4c**) and 489 tissue-specific chromatin states^{29,30} (**Fig. 4d**).

We found significant heritability enrichment in oligodendrocytes (P-value=0.03), a specific type of neuroglial cells, for the brain BAG. The cardiovascular BAG also exhibited significant heritability enrichment in neurons (P-value=0.01) (**Fig. 4a, Supplementary eFile 9**). Concerning the heritability enrichment in non-tissue-specific functional categories, we exemplified the four highest significant partitioned heritability estimates for each BAG in **Fig. 4b**. For the brain BAG, the super-enhancer regions employed 17.16% of SNPs to explain 0.47 ± 0.04 of SNP heritability (P-value= 1.80×10^{-11}), and the histone H3 at lysine 9 (H3K9ac) regions used 12.61% of SNPs to explain 0.61 ± 0.12 of SNP heritability (P-value= 2.96×10^{-4}). For the eye BAG, the super-enhancer regions explained 0.39 ± 0.05 of SNP heritability (P-value= 2.12×10^{-6}) using 16.84% of SNPs. For the hepatic BAG, the H3K9ac regions explained 0.69 ± 0.13 of SNP heritability (P-value= 3.60×10^{-5}) using 12.61% of SNPs. For the immune BAG, the TSS regions (i.e., core promoters) explained 0.37 ± 0.08 of SNP heritability (P-value= 1.48×10^{-6}) using 1.82% of SNPs. The 3.11% of SNPs annotated by the promoter regions explained 0.30 ± 0.08 of SNP heritability (P-value= 7.64×10^{-4}) for the metabolic BAG. For the cardiovascular (enrichment= 16.39 ± 2.23 ; P-value= 4.70×10^{-11}), musculoskeletal (enrichment= 17.34 ± 4.08 ; P-value= 1.65×10^{-6}), pulmonary (enrichment= 16.82 ± 2.51 ; P-value= 7.58×10^{-9}), and renal (enrichment= 13.96 ± 1.88 ; P-value= 7.25×10^{-9}) BAGs, the highest heritability enrichment was found in the regions conserved across mammals (**Fig. 4b, Supplementary eFile 10**). These results suggested disproportionate genomic contributions to the heritability of BAGs from multiple functional categories.

In addition, the nine BAGs showed high heritability enrichment in specific tissues corresponding to their organ systems. For example, the cardiovascular BAG showed significant heritability enrichment in multiple tissue types, including the artery (e.g., the aorta: P-value= 1.03×10^{-7}), myometrium (P-value= 1.35×10^{-4}), and uterus (P-value= 2.43×10^{-4}). Significant heritability enrichment was found in the liver for the hepatic (P-value= 5.60×10^{-9}) and metabolic BAGs (P-value= 6.24×10^{-9}). For the immune BAG, significant heritability enrichment was found in fetal blood tissues (P-value= 7.36×10^{-9}) (**Fig. 4c, Supplementary eFile 11**). These findings were aligned with the tissue-specific gene expression patterns observed at the gene level (**Fig. 3b**).

The results from multi-tissue chromatin states-specific data further provide the proof-of-concept for the organ-specific heritability enrichment among these nine BAGs. For the brain BAG, significant heritability enrichment was found in multiple brain tissues in the H3K4me3 (e.g., P-value= 9.06×10^{-5} for the hippocampus), H3K4me1 (e.g., P-value= 6.94×10^{-5} for the hippocampus), and H3K27ac (e.g., P-value= 1.15×10^{-5} for the anterior caudate) regions. For the cardiovascular BAG, significant heritability enrichment was shown in the right ventricle in the

H3K4me3 region (P -value= 6.36×10^{-5}) and the artery aorta in the H3K27ac region (P -value= 5.81×10^{-7}). Significant heritability enrichment was found in primary hematopoietic stem cells in the H3K4me1 region for the immune BAG for both females (P -value= 5.61×10^{-5}) and males (P -value= 9.50×10^{-5}). The fetal leg muscle tissue in the DNase regions (P -value= 6.54×10^{-5}) for the musculoskeletal BAG showed significant heritability enrichment. For the pulmonary BAG, significant heritability enrichment was found in the fetal lung in the H3K4me1 (P -value= 1.33×10^{-9}) and DNase regions (P -value= 3.80×10^{-8}), among other tissues from the stomach, artery, and muscle. For the renal BAG, significant enrichment was shown in the liver in the H3K9ac region (P -value= 2.46×10^{-5}) and the gastric tissues in the H3K27ac region (P -value= 6.24×10^{-5}) (Fig. 4d, Supplementary eFile 12).

Cheverud's Conjecture: genetic correlations between the nine biological age gaps mirror their phenotypic correlations

We estimated the genetic correlation (g_c) (Method 2h) and the phenotypic correlation (p_c for Pearson's correlation coefficient) between each pair of the nine BAGs. Our results supported the long-standing Cheverud's Conjecture¹ – the genetic correlation between two clinical traits reflects their phenotypic correlation (Fig. 4e).

The musculoskeletal and hepatic BAGs showed the highest genetic correlation ($g_c=0.40$) and phenotypic correlation ($p_c=0.38$). Similarly, the hepatic and renal BAGs showed a high genetic correlation ($g_c=0.39$) and phenotypic correlation ($p_c=0.37$). The musculoskeletal BAG also showed significant genetic and phenotypic correlations with pulmonary ($g_c=0.35$, $p_c=0.19$) and renal BAGs ($g_c=0.13$, $p_c=0.21$). In addition, the eye BAG showed small genetic and phenotypic correlations with the brain BAG ($g_c=0.15$, $p_c=0.11$). The correlations between the brain and eye BAGs and other organ BAGs were relatively weaker than those observed among other organ pairs. These findings indicate the presence of shared genetic underpinnings that collectively contribute to the biological aging processes captured by these organ BAGs. Detailed results are presented in Supplementary eFile 13.

Genetic correlations between the nine biological age gaps and 41 clinical traits of chronic diseases, cognition, and lifestyle factors

We also estimated g_c between the nine BAGs and 41 clinical traits to examine their genetic correlations. The 41 clinical traits encompassed many common chronic diseases and conditions and their disease subtypes^{7,31–34}, cognition (e.g., general intelligence and reaction time, and lifestyle factors (e.g., computer use) (Fig. 4f and Supplementary eTable 2).

The brain BAG was genetically associated with several brain diseases of the central nervous system (CNS) and their subtypes, including AD ($g_c=0.37 \pm 0.14$) and late-life depression (LLD, $g_c=0.25 \pm 0.07$). Furthermore, we observed significant genetic correlations between the brain BAG and years of education ($g_c=-0.14 \pm 0.05$) and intelligence ($g_c=-0.15 \pm 0.05$). The cardiovascular BAG was positively correlated with stroke ($g_c=0.20 \pm 0.05$), a significant cardiovascular disease, and was negatively correlated with years of education ($g_c=-0.17 \pm 0.05$). The musculoskeletal BAG was positively correlated with hyperlipidemia ($g_c=0.18 \pm 0.06$), rheumatoid arthritis ($g_c=0.13 \pm 0.03$), and Crohn's disease ($g_c=0.19 \pm 0.06$) and was negatively

correlated with atrial fibrillation ($g_c = -0.11 \pm 0.04$), years of education ($g_c = -0.21 \pm 0.04$), and intelligence ($g_c = -0.18 \pm 0.03$). The pulmonary BAG was positively associated with hyperlipidemia ($g_c = 0.12 \pm 0.04$), stroke ($g_c = 0.15 \pm 0.05$), liver fat ($g_c = 0.12 \pm 0.04$), and lung carcinoma ($g_c = 0.17 \pm 0.05$). Finally, the renal BAG was positively correlated with chronic kidney disease ($g_c = 0.39 \pm 0.06$) and atrial fibrillation ($g_c = 0.09 \pm 0.03$). Notably, type 2 diabetes showed abundant positive genetic correlations with multiple BAGs, including the brain, cardiovascular, metabolic, pulmonary, and renal. Detailed results are presented in **Supplementary eFile 14**.

These genetic correlations yield insights into potential shared mechanisms underlying the nine BAGs, their relationships with chronic diseases, particularly AD and type 2 diabetes, and cognition. These compelling results prompted us to explore the potential causal effects of these traits on the nine BAGs. In the subsequent section, we unbiasedly selected 17 clinical traits encompassing chronic diseases, cognition, and lifestyle factors to perform Mendelian randomization (**Method 2g**).

purposes. **c)** Tissue-specific partitioned heritability estimates using gene sets from multi-tissue gene expression data. **d)** Tissue and chromatin-specific partitioned heritability estimates using multi-tissue chromatin data. **e)** Cheverud's Conjecture: the genetic correlation between two BAGs (g_c , lower triangle) mirrors their phenotypic correlation (p_c , upper triangle). **f)** Genetic correlations between the nine BAGs and 41 clinical traits, including chronic diseases and their subtypes involving multiple human organ systems, education, intelligence, and reaction time. The symbol * denotes Bonferroni-corrected significance; the absence of * indicates all results remain significant after correction. The standard error of the estimated parameters is presented using error bars. Abbreviation: AD: Alzheimer's disease; ASD: autism spectrum disorder; LLD: late-life depression; SCZ: schizophrenia; DB: type 2 diabetes; WMH: white matter hyperintensity; HPLD: hyperlipidemia; AF: atrial fibrillation; RA: rheumatoid arthritis; CD: Crohn's disease; CKD: chronic kidney disease.

Hepatic and musculoskeletal biological age gaps are causally associated with each other

We performed two-sample bi-directional Mendelian randomization for each pair of BAGs by excluding overlapping populations to avoid bias¹⁶ (**Method 2j**). We found that the hepatic and musculoskeletal BAGs showed a bi-directional causal relationship [from the hepatic BAG to the musculoskeletal BAG: $P\text{-value}=9.85 \times 10^{-7}$, OR (95% CI) = 1.47 (1.26, 1.71); from the musculoskeletal BAG to the hepatic BAG: $P\text{-value}=1.54 \times 10^{-8}$, OR (95% CI) = 2.78 (1.95, 3.97)] (**Fig. 5**). This causal relationship echoes our genetic correlation results: the musculoskeletal and hepatic BAGs showed the highest genetic correlation compared to other organ systems (**Fig. 4e**). Detailed results are presented in **Supplementary eFile 15** for the Mendelian randomization and **Supplementary eFigure 14** and **15** for the sensitivity check.

Biological age gaps are causally associated with several chronic diseases, body weight, and sleep duration

We investigated the bi-directional causal effects between chronic diseases (e.g., AD) and lifestyle factors (e.g., sleep duration) and the nine BAGs. We unbiasedly and systematically included 17 clinical traits (**Method 2j**) guided by our genetic correlation results (**Fig. 4f**). The 17 clinical traits included chronic diseases linked to the brain, cardiovascular, metabolic, digestive, renal, and musculoskeletal systems, cognition, and lifestyle factors (**Supplementary eTable 3**).

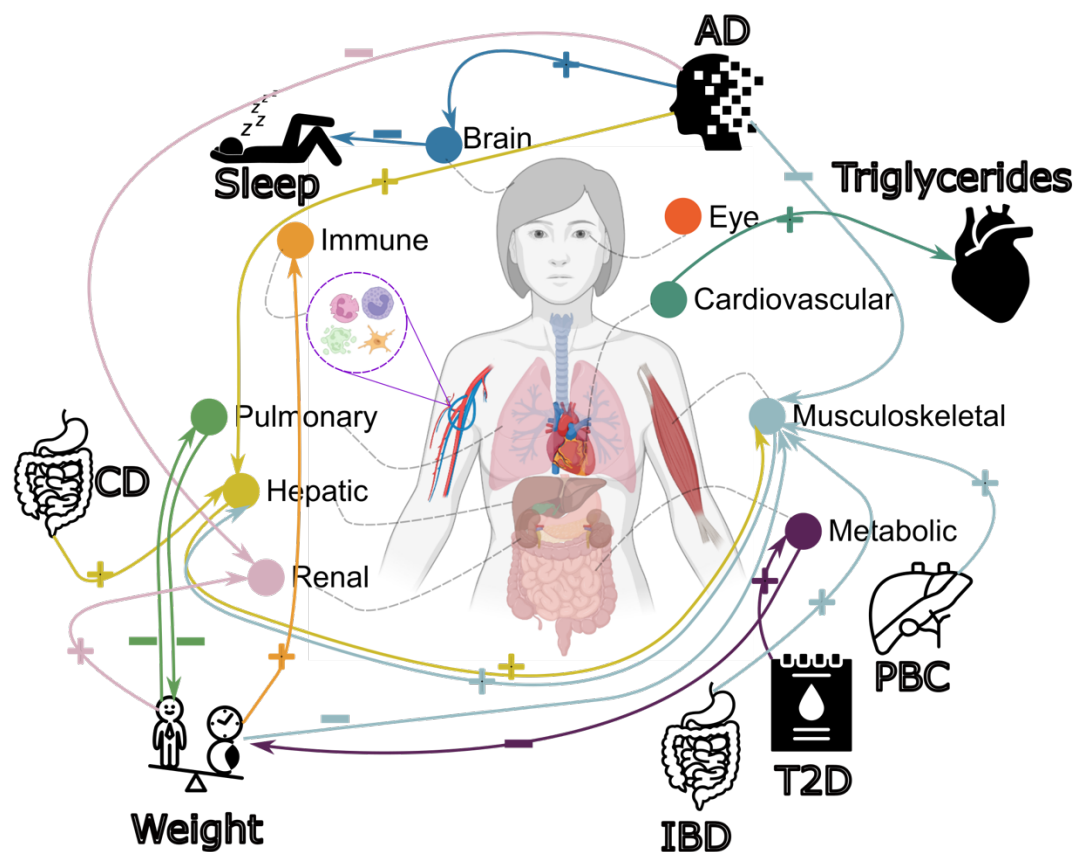
In the forward Mendelian randomization, we found potential causal effects of AD on the brain [$P\text{-value}=3.99 \times 10^{-8}$, OR (95% CI) = 1.05 (1.03, 1.06), number of SNPs=10], hepatic [$P\text{-value}=7.53 \times 10^{-7}$, OR (95% CI) = 1.03 (1.02, 1.04), number of SNPs=10], musculoskeletal [$P\text{-value}=1.73 \times 10^{-5}$, OR (95% CI) = 0.98 (0.97, 0.99), number of SNPs=10], and renal [$P\text{-value}=5.71 \times 10^{-4}$, OR (95% CI) = 0.98 (0.97, 0.99), number of SNPs=10] BAGs. Body weight showed causal effects on multiple organ systems, including the immune [$P\text{-value}=8.96 \times 10^{-5}$, OR (95% CI) = 1.08 (1.04, 1.11), number of SNPs=160], musculoskeletal [$P\text{-value}=4.32 \times 10^{-15}$, OR (95% CI) = 0.83 (0.79, 0.86), number of SNPs=160], pulmonary [$P\text{-value}=3.50 \times 10^{-7}$, OR (95% CI) = 0.84 (0.79, 0.90), number of SNPs=160], and renal BAGs [$P\text{-value}=4.53 \times 10^{-13}$, OR (95% CI) = 1.18 (1.13, 1.23), number of SNPs=160]. In addition, we also found that Crohn's disease had causal effects on the hepatic BAG [$P\text{-value}=3.00 \times 10^{-3}$, OR (95% CI) = 1.02 (1.00, 1.03), number of SNPs=77], type 2 diabetes on the metabolic BAG [$P\text{-value}=9.92 \times 10^{-12}$, OR (95% CI) = 1.16 (1.09, 1.24), number of SNPs=8], inflammatory bowel disease [$P\text{-value}=1.42 \times 10^{-3}$, OR

(95% CI) = 1.02 (1.00, 1.03), number of SNPs=80] and primary biliary cholangitis [P-value= 7.41×10^{-4} , OR (95% CI) = 1.02 (1.00, 1.03), number of SNPs=16] on the musculoskeletal BAG (**Fig. 5**).

For the inverse Mendelian randomization, we found potential causal effects of the metabolic [P-value= 6.85×10^{-4} , OR (95% CI) = 0.94 (0.91, 0.97), number of SNPs=71] and pulmonary [P-value= 3.79×10^{-5} , OR (95% CI) = 0.84 (0.79, 0.91), number of SNPs=62] BAGs on body weight, the cardiovascular BAG on triglycerides versus lipid ratio in very large very-low-density lipoprotein (VLDL) [P-value= 2.14×10^{-4} , OR (95% CI) = 1.09 (1.04, 1.14), number of SNPs=39], and the brain BAG on sleep duration [P-value= 2.61×10^{-3} , OR (95% CI) = 1.09 (1.04, 1.14), number of SNPs=10] (**Fig. 5**). Detailed results are presented in **Supplementary eFile 16**.

We performed several sensitivity analyses (**Method 2j**) to test the robustness of our findings. Based on these sensitivity checks, we found outlier instrumental variables (IVs, i.e., SNPs) for four Mendelian randomization tests (AD and body weight on musculoskeletal BAG, Crohn's disease on hepatic BAG, and type 2 diabetes on metabolic BAG) in the forward Mendelian randomization and one Mendelian randomization test (metabolic BAG on body weight) in the inverse Mendelian randomization. We reran the analyses by excluding these outlier SNPs, and the results remained consistent. Detailed results of the sensitivity check are presented in **Supplementary eFigure 16-31** for all significant results.

Figure 5: Causal multi-organ network between the 9 biological age gaps and 17 clinical traits of chronic diseases, lifestyle factors, and cognition



We conducted two sets of Mendelian randomization analyses. Firstly, we examined the causal relationships between each pair of BAGs, excluding overlapping populations. Secondly, we investigated the causal associations between the 9 BAGs and the 17 unbiasedly selected clinical traits. Bi-directional analyses, including forward and inverse analyses on the exposure and outcome variables, were performed in all experiments. Significant tests were adjusted for multiple comparisons using the Bonferroni correction. Each colored arrow represents a potential causal effect connecting the exposure variable to the outcome variable. The symbol "+" denotes an OR larger than 1, while "-" represents an OR smaller than 1. Detailed OR and 95%CI information can be found in **Supplementary eFigure 32** and **eFile 15-16**. Abbreviation: AD: Alzheimer's disease; T2D: type 2 diabetes; PBC: primary biliary cholangitis; CD: Crohn's disease; IBD: inflammatory bowel disease; CI: confidence interval; OR: odds ratio.

Discussion

The current study comprehensively depicts the genetic architecture of common genetic variants on biological aging of nine human organ systems using multimodal data from 377,028 European ancestry participants. We identified many (143 novel) genomic loci for the BAGs of nine human organ systems, which exhibited significant associations with a wide range of clinical traits documented in the GWAS Catalog. These associations were observed within a phenotypic landscape characterized by BAG-organ specificity and inter-organ crosstalk. The brain BAG showed the highest SNP-based heritability estimate among all nine organ systems. GESA, tissue-specific gene expression patterns, and heritability enrichment results provided additional evidence supporting biological validation for BAG-organ specificity and inter-organ crosstalk. The phenotypic correlation between BAGs was a proxy for their genetic correlation, thereby supporting the long-standing Cheverud's Conjecture. Mendelian randomization demonstrated potential causal relationships between chronic diseases, particularly AD and type 2 diabetes, body weight, sleep duration, and the nine BAGs.

Our large-scale multi-organ GWAS significantly expands the current catalog of genetic variants associated with health-related traits. The discovery of the 143 novel genomic loci has significant clinical implications. These findings provide an invaluable foundation to validate genes or regulatory elements, molecular pathways, and biological processes related to the clinical traits and diseases of interest in the current study and future GWAS analyses. Previous GWAS mainly focused on the BAG in one organ system, such as the brain BAG^{14,35–37} from imaging-derived phenotypes. These investigations have largely overlooked the inherent interconnectedness of human organ systems, which are intricately intertwined with distinct axes. Recent studies have identified notable axes, such as the heart-brain-liver¹¹, brain-eye³⁸, and brain-heart³⁹ axes, highlighting the importance of comprehending these intricate relationships to understand human physiology and health.

Our phenome-wide associations validate the pleiotropic effects of the identified genomic loci, influencing various health-related clinical traits in the GWAS Catalog. Our findings also highlight BAG-organ specificity and inter-organ crosstalk, further supporting that biological aging is a complex, multifaceted phenomenon. The human brain regulates various physiological processes and maintains homeostasis throughout the body. Consequently, it is unsurprising that the brain exhibits interconnectedness with clinical traits associated with multiple organ systems. The remarkable enrichment of metabolic traits across various organ systems is unsurprising. As a vital metabolic organ, the liver substantially overlaps genetic variants and loci with both the hepatic and metabolic BAGs. Biologically, the liver's metabolic functions are intricately regulated by hormones like insulin and other metabolic regulators¹². Similarly, the interplay between immune and metabolic processes is essential for maintaining overall health and is crucial for the body's ability to respond to pathogens and regulate metabolic homeostasis⁶.

We highlighted that the brain BAG is the most heritable among the nine organ systems. Determining the genetic heritability of specific organ systems can be complex as no organ system functions independently, and many diseases or traits involve complex interactions between multiple organ systems, as well as genetic and environmental factors. The brain plays a crucial role in developing and functioning various physiological processes across the body. Its intricate structure and diverse cell types render it vulnerable to genetic influences⁴⁰. Therefore, the brain may exhibit higher genetic stability and less environmental variability⁴¹ than other organs. The human brain's extensive functional connectivity and intricate networks may also contribute to its higher heritability. These networks facilitate the transmission of genetic

information and the propagation of genetic effects across different brain regions⁴². Lastly, genetic variations shaping the human brain are pleiotropic and influence cognitive abilities, behavior, and susceptibility to neurological and psychiatric disorders. Collectively, these factors may contribute to the marked genetic heritability observed in the human brain compared to other organ systems.

Our gene-level and partitioned heritability analyses further validate our GWAS findings, supporting BAG-organ specificity and inter-organ crosstalk. In GSEA, the genes associated with the cardiovascular BAG were implicated in the IGF-II pathway. IGF-II activates two receptors (IGF-1R and IR-A) to promote cell growth and survival. The IGF signaling pathway is essential for cardiac development in the human heart - the first functional organ to develop⁴³. In particular, IGF-II promotes fetal cardiomyocyte proliferation through the tyrosine kinase receptors IGF1R and INSR. Previous research provided appealing evidence on IGF signaling in cardiac regeneration in animal models and induced pluripotent stem cells⁴⁴. The flavonoid glucuronidation pathway was the most significant enrichment result shown in the hepatic BAG. A previous study demonstrated that procyanidin C1, a flavonoid in grape seed extract, extended the lifespan of mice⁴⁵. Furthermore, ample evidence indicated that natural flavonoids could be potential therapeutic approaches for non-alcoholic fatty liver disease⁴⁶. The metabolites formed through this pathway can also exert effects beyond the liver and impact other organ systems. Our tissue-specific gene expression analyses provided additional support for the biological relevance of our GWAS findings, as the identified genes exhibited specific expression patterns within tissues from the corresponding organ systems.

The heritability enrichment analysis further validates the BAG-organ specificity and inter-organ connections by highlighting the disproportional heritability enrichment of genetic variants in different functional categories, cell types, tissues, and chromatin states. The cell type-specific enrichment results in the brain (i.e., oligodendrocytes) and cardiovascular (i.e., neurons) BAGs align with previous research. Specifically, Zhao et al. conducted a large-scale GWAS on brain white matter microstructure and found significant heritability enrichment in glial cells, particularly oligodendrocytes⁴⁷, which aligns with our current findings. Our previous multimodal brain BAG GWAS¹⁴ also confirmed this enrichment in the brain BAG derived from the white matter microstructural features. Similarly, research has revealed the presence of an "intrinsic cardiac nervous system" within the heart, often called the "heart brain." This system consists of around 40,000 neurons similar to those found in the brain, indicating that the heart possesses a distinct nervous system⁴⁸.

Our genetic correlation results confirmed that the genetic correlation generally mirrors phenotypic correlations in multi-organ biological age. This suggests that environmental factors likely affect the aging of multiple organ systems in the same direction. Providing evidence for Cheverud's Conjecture can have clinical implications by providing valuable insights into the genetic basis of complex age-related diseases. For instance, by identifying the shared genetic factors underlying multiple age-related diseases, we can target these common pathways to develop novel treatments or repurpose existing drugs⁴⁹ that have proven efficacy in one disease or condition for treating others. Moreover, the validation of Cheverud's Conjecture emphasizes the importance of considering the genetic covariance of age-related diseases in clinical practice. It underscores the need for comprehensive genetic assessments and genomic analyses to understand disease risk and progression⁵⁰.

We found a bi-directional causal relationship between the hepatic and musculoskeletal BAGs. Abundant research has suggested that liver function and metabolic health, particularly

related to glucose and lipid metabolism, can significantly impact musculoskeletal health⁵¹. This inter-organ crosstalk can cause dysregulation of liver metabolism (e.g., non-alcoholic fatty liver disease) linked to musculoskeletal disorders, including osteoporosis, sarcopenia, and muscle wasting. The musculoskeletal system can also exert an inverse influence on liver function. Regular physical activity and muscle strength have been linked to enhanced liver health and decreased susceptibility to liver diseases. To further support this, causal effects of primary biliary cholangitis, a chronic liver disease, on elevated musculoskeletal BAG were confirmed in our Mendelian randomization results (**Fig. 5**). The absence of direct causal relationships between the remaining BAGs can be attributed to various factors with potential explanations and implications. One possible explanation is that the brain BAG, having the smallest sample size in our GWAS (after removing overlapping participants), may be limited in statistical power. In addition, this may suggest that various factors, including chronic diseases, environmental exposures, and lifestyle choices, influence biological aging in alternative pathways or mediate such changes. Thus, understanding the collective contribution of chronic diseases, environmental factors, and lifestyle choices is crucial for comprehending the overall aging process and its impact on organ health.

We found that several clinical traits collectively cause organ systems to appear older or younger than their chronological age. For instance, body weight was causally associated with the immune, musculoskeletal, metabolic, and pulmonary BAGs. For several reasons, body weight can causally influence multiple organ systems. Excessive body weight (e.g., obesity) has metabolic consequences, including increased inflammation, insulin resistance, and dysregulation of metabolic pathways in adipose tissue⁵². It also leads to mechanical stress on the body, contributing to musculoskeletal strain⁵³ and cardiovascular workload⁵⁴. Hormonal imbalances⁵⁵ and lifestyle factors linked to body weight also influence multi-organ function and the development of chronic diseases. Being overweight is also a risk factor for type 2 diabetes, which was positively causally associated with metabolic BAG (**Fig. 5**). AD was causally linked to the brain, hepatic, musculoskeletal, and renal BAGs. AD, a neurodegenerative disorder primarily affecting the brain, can have causal influences on multiple organ systems. For example, it has broader systemic involvement beyond the brain, mediated by mechanisms including protein aggregation (e.g., amyloid- β and tau⁵⁶), vascular dysfunction⁵⁷, inflammation⁵⁸, and other secondary factors. Protein aggregates can spread to other organs; vascular abnormalities can impact blood flow; inflammation can affect distant organ systems; secondary factors, such as medication use and lifestyle changes, also contribute.

In conclusion, our study presents compelling genetic evidence to support that *no organ system is an island*¹ – the collective influence of various chronic diseases on these multi-organ systems and the interconnectedness among these human organ systems. These findings highlight the importance of comprehensively understanding the underlying causes of chronic diseases within the multi-organ network. By shedding light on its comprehensive genetic architecture, our study paves the way for future research to unravel complex disease mechanisms and develop holistic approaches to ameliorate overall organ health.

¹ We adapt the concept of "No Man Is An Island" from the poem by John Donne, highlighting the interconnectedness of human organ systems.

Methods

Method 1: Study populations

UKBB is a population-based study of approximately 500,000 people recruited between 2006 and 2010 from the United Kingdom. The UKBB study has ethical approval, and the ethics committee is detailed here: <https://www.ukbiobank.ac.uk/learn-more-about-uk-biobank/governance/ethics-advisory-committee>.

The current study analyzed multimodal data, including imaging-derived phenotypes (IDP) and physical and physiological measures in nine human organ systems from 154,774 UKBB participants. In our previous study, we constructed BAGs for eight organ systems using machine learning, including MRI data for brain BAG from 30,108 participants (European ancestry), pulse rate and blood pressure data for cardiovascular BAG, liver-related blood biomarkers for hepatic BAG, C-reactive protein and blood hematology variables for immune BAG, blood biomarkers for metabolic BAG, physical measurements and vitamin D for musculoskeletal BAG, lung functioning measurements for pulmonary BAG, and glomerular filtration and electrolyte regulation biomarkers for renal BAG from 111,543 participants. Furthermore, the current study also used 60 optical coherence tomography (OCT)-derived measures from 36,004 participants to derive the BAG of the ninth organ system – the eye BAG. The inclusion criteria for the features used to predict the eight BAGs, the machine learning methods, and cross-validation procedures are detailed in our previous study³. We initially used the 88 OCT-derived measures (category ID: 10079) for the additional eye BAG in 67,549 participants. Of these measures, 28 were excluded due to a high missing rate (>20% of participants). Additionally, 4172 participants were excluded due to missing data, and 1798 participants identified as outliers (outside mean \pm 6SD) for the 60 remaining measures were discarded. This finally resulted in 41,966 participants (36,004 European ancestry participants). The included 2444 features to derive the BAG of the nine organ systems are presented in **Supplementary eFile 17**.

In addition, we also performed GWAS for seven variables from 222,254 UKBB participants by excluding the 154,774 participants from the BAG populations to avoid bias due to overlapping samples. These variables included six lifestyle factors and one cognitive variable: $N=219,661$ (European ancestry) for coffee intake (Field ID:1498), $N=221,393$ for fresh fruit intake (Field ID:1309), $N=221,739$ for tea intake (Field ID:1488), $N=220,765$ for sleep duration (Field ID:1160), $N=209,012$ for time spent outdoors in summer (Field ID:1050), $N=221,337$ for body weight (Field ID:21002), and $N=220,624$ for reaction time (Field ID:20023).

The current work was jointly performed under application numbers 35148 (i.e., genetic data) and 60698 (i.e., the generation of the nine BAGs). In total, we analyzed data from 377,028 individuals of European ancestry in the current study.

Method 2: Genetic analyses

We used the imputed genotype data for all genetic analyses, and our quality check pipeline resulted in 487,409 participants and 6,477,810 SNPs. After merging with the population for each BAG, we included 30,108-111,543 European ancestry participants for the nine BAGs (**Fig. 1**). To avoid bias due to overlapping populations¹⁶, we also used the rest of the UKBB participants of European ancestry (non-overlapping) to derive the GWAS summary statistics for several

lifestyle factors (**Method 2j**). Details of the genetic quality check protocol are described elsewhere^{32,59}.

(a): Genome-wide association analysis: For GWAS, we ran a linear regression using Plink⁶⁰ for each BAG, controlling for confounders of age, dataset status (training/validation/test or independent test dataset), age x squared, sex, age x sex interaction, age-squared x sex interaction, and the first 40 genetic principal components; additional covariates for total intracranial volume and the brain position in the scanner were included for brain BAG GWAS. We adopted the genome-wide P-value threshold (5×10^{-8}) and annotated independent genetic signals considering linkage disequilibrium (see below). To check the robustness of our GWAS results, we also performed sex-stratified GWAS for males and females and split-sample GWAS by randomly dividing the entire population into two splits (sex and age-matched).

(b): SNP-based heritability: We estimated the SNP-based heritability (h^2) using GCTA⁶¹ with the same covariates in GWAS. We reported results from two experiments for each BAG using *i*) the full sample sizes and *ii*) randomly down-sampled sample sizes to that ($N=30,108$) of the brain BAG with comparable distributions regarding sex and age – the sample size of brain BAGs was smaller than the other BAGs.

(c): Annotation of genomic loci: The annotation of genomic loci and mapped genes was performed via FUMA⁶². For the annotation of genomic loci, FUMA first defined lead SNPs (correlation $r^2 \leq 0.1$, distance < 250 kilobases) and assigned them to a genomic locus (non-overlapping); the lead SNP with the lowest P-value (i.e., the top lead SNP) was used to represent the genomic locus. For gene mappings, three different strategies were considered. First, positional mapping assigns the SNP to its physically nearby genes (a 10 kb window by default). Second, eQTL mapping annotates SNPs to genes based on eQTL associations using the GTEx v8 data. Finally, chromatin interaction mapping annotates SNPs to genes when there is a significant chromatin interaction between the disease-associated regions and nearby or distant genes⁶². The definition of top lead SNP, lead SNP, independent significant SNP, and candidate SNP can be found in **Supplementary eMethod 2**.

(d): Phenome-wide associations for the identified SNPs: We queried the candidate and significant independent SNPs within each locus in the EMBL-EBI GWAS Catalog to determine their previously identified associations with any other traits. For these associated traits, we further mapped them into organ-specific groups and other chronic disease traits and cognition for visualization purposes.

(e): Gene set enrichment analysis: We first performed gene-level association analysis using MAGMA²⁰. First, gene annotation was performed to map the SNPs (reference variant location from Phase 3 of 1,000 Genomes for European ancestry) to genes according to their physical positions. We then performed gene-level associations based on the SNP GWAS summary statistics to obtain gene-level p-values between the nine BAGs and the curated protein-encoding genes containing valid SNPs. We performed GSEA using the gene-level association p-values. Gene sets were obtained from the Molecular Signatures Database (MsigDB, v7.5.1)⁶³, including 6366

curated and 10,402 ontology gene sets. All other parameters were set by default for MAGMA. The Bonferroni method was used for correcting multiple comparisons for all tested gene sets.

(f): Tissue-specific gene expression analysis: MAGMA performed gene-property analyses to identify tissue-specific gene expression of the nine BAGs. The gene-property analysis converts the gene-level association P-values (above) to Z scores and tests a specific tissue's gene expression value versus the average expression value across all tissues in a regression model. Bonferroni correction was performed for all tested gene sets. We reported the results from the 54 tissue types using the GTEx V8 data.

(g): Gene-drug-disease network: We tested the enrichment of the nine BAG-linked genes in the targeted gene sets for different drug categories from the DrugBank database²⁵. The gene-drug-disease network was constructed to prioritize potentially repositionable drugs. The GREP software²⁴ performs Fisher's exact tests to examine whether the prioritized genes are enriched in gene sets targeted by drugs in a clinical indication category for a certain disease or condition. Bonferroni correction was performed for all tested drugs.

(h): Genetic correlation: We used the LDSC⁶⁴ software to estimate the pairwise genetic correlation (g_c) between each pair of BAGs, as well as between the nine BAG and 41 other clinical traits, including chronic diseases involving multiple organ systems, such as AD for brain and chronic kidney disease for kidney, cognition, and lifestyle factors. We used the precomputed LD scores from the 1000 Genomes of European ancestry. To ensure the suitability of the GWAS summary statistics, we first checked that the selected study's population was European ancestry; we then guaranteed a moderate SNP-based heritability h^2 estimate. Notably, LDSC corrects for sample overlap and provides an unbiased estimate of genetic correlation⁵⁰. The inclusion criteria and finally included traits are detailed in **Supplementary eTable 2**. Bonferroni correction was performed for the 41 clinical traits.

(i): Partitioned heritability estimate: Partitioned heritability analysis estimates the percentage of heritability enrichment explained by pre-defined, annotated genome regions and categories²⁷. First, the partitioned heritability was calculated for 53 general functional categories (one including the entire set of SNPs). The 53 functional categories are not specific to any cell type and include coding, UTR, promoter and intronic regions, etc. The details of the 53 categories are described elsewhere²⁷. Subsequently, cell and tissue type-specific partitioned heritability was estimated using gene sets from Cahoy et al.²⁸ for three main cell types (i.e., astrocyte, neuron, and oligodendrocyte), multi-tissue chromatin states-specific data (ROADMAP²⁹ and ENTE³⁰), and multi-tissue gene expression data (GTEx V8²³). Bonferroni correction was performed for all tested annotations and categories.

(j): Two-sample bi-directional Mendelian randomization: We investigated whether one BAG was causally associated with another BAG and whether the 41 clinical traits were causally associated with the nine BAGs (**Fig. 4**). To this end, we employed a bidirectional, two-sample Mendelian randomization using the TwoSampleMR package⁶⁵. Both the forward and inverse Mendelian randomization were performed between each pair of traits by switching the exposure and outcome variables. We applied five different Mendelian randomization methods and

reported the results of inverse variance weighted (IVW) in the main text and the four others (i.e., Egger, weighted median, simple mode, and weighted mode estimators) in the supplement.

For the causal inference of each pair of BAGs, all GWAS summary statistics were derived from our analyses by excluding overlapping populations of the two BAGs. For example, to test the causal relationship between the brain BAG and cardiovascular BAG, we reran GWAS for the cardiovascular BAG by excluding the partially overlapping population from the brain BAG. For all the seven body organ systems which had entirely overlapping populations, we used the GWAS data from the split-sample analyses (**Method 2a**). For instance, the GWAS for the cardiovascular BAG was from the first-split data, and the pulmonary BAG was from the second-split data. Bonferroni correction was performed for the tested BAGs.

One key challenge in our hypothesis-driven Mendelian randomization is to select these exposure variables unbiasedly. Clinical traits sharing common genetic covariance with nine BAGs are more likely to be causally associated with them. We performed a systematic inclusion procedure using the following criteria to overcome this. We manually queried the 41 clinical traits – used in our genetic correlation analyses – in the IEU GWAS database, specifically curated for Mendelian randomization analyses. We ranked all available studies for a certain trait (e.g., AD) based on the sample sizes. We then chose the study whose populations were of European ancestry and did not include UKBB participants to avoid bias due to overlapping populations¹⁶. For the traits whose GWAS data were available in the IEU GWAS database, we used the TwoSampleMR package to perform the Mendelian randomization analysis. For the traits whose data were not appropriate in the IEU GWAS database, we then performed another manual query in the EMBL-EBI GWAS Catalog database to download the available GWAS summary statistics with the same filter criteria. For the traits whose GWAS data were dominated by studies using UKBB participants in both databases, we ran GWAS using our own UKBB data by excluding overlapping populations. Finally, after harmonizing their GWAS summary statistics, this resulted in 17 clinical traits with at least eight valid IVs (i.e., SNPs). The 17 clinical traits included chronic diseases affecting multiple organ systems, cognition, and lifestyle factors (**Supplementary eTable 3**). Bonferroni correction was performed for all tested clinical traits.

We performed several sensitivity analyses. First, a heterogeneity test was performed to check for violating the IV assumptions. Horizontal pleiotropy was estimated to navigate the violation of the IV's exclusivity assumption⁶⁶ using a funnel plot, single-SNP Mendelian randomization approaches, and Mendelian randomization Egger estimator⁶⁷. Moreover, the leave-one-out analysis excluded one instrument (SNP) at a time and assessed the sensitivity of the results to individual SNP.

Data Availability

The GWAS summary statistics corresponding to this study are publicly available on the MEDICINE knowledge portal (<https://labs.loni.usc.edu/medicine>), the FUMA online platform (<https://fuma.ctglab.nl/>), the EMBL-EBI GWAS Catalog platform (<https://www.ebi.ac.uk/gwas/home>), and the IEU GWAS database (<https://gwas.mrcieu.ac.uk/>).

Code Availability

The software and resources used in this study are all publicly available:

- MEDICINE: <https://labs.loni.usc.edu/medicine>, knowledge portal for dissemination
- BioAge: <https://github.com/yetianmed/BioAge>, biological age prediction
- PLINK: <https://www.cog-genomics.org/plink/>, GWAS
- FUMA: <https://fuma.ctglab.nl/>, gene mapping, genomic locus annotation
- GCTA: <https://yanglab.westlake.edu.cn/software/gcta/#Overview>, heritability estimates
- LDSC: <https://github.com/bulik/ldsc>, genetic correlation and partitioned heritability
- TwoSampleMR: <https://mrcieu.github.io/TwoSampleMR/index.html>, Mendelian randomization

Competing Interests

None

Authors' contributions

Dr. Wen has full access to all the data in the study and takes responsibility for the integrity of the data and the accuracy of the data analysis.

Study concept and design: Wen

Acquisition, analysis, or interpretation of data: Wen, Tian, Zalesky, Davatzikos

Drafting of the manuscript: Wen, Tian, Zalesky, Davatzikos

Critical revision of the manuscript for important intellectual content: all authors

Statistical analysis: Wen

BAG index generation: Tian

References

1. Cheverud, J. M. A COMPARISON OF GENETIC AND PHENOTYPIC CORRELATIONS. *Evolution* **42**, 958–968 (1988).
2. Melzer, D., Pilling, L. C. & Ferrucci, L. The genetics of human ageing. *Nat Rev Genet* **21**, 88–101 (2020).
3. Tian, Y. E. *et al.* Heterogeneous aging across multiple organ systems and prediction of chronic disease and mortality. *Nat Med* 1–11 (2023) doi:10.1038/s41591-023-02296-6.
4. Cohen, A. A. *et al.* A complex systems approach to aging biology. *Nat Aging* **2**, 580–591 (2022).
5. Hodson, R. Precision medicine. *Nature* **537**, S49–S49 (2016).
6. Hotamisligil, G. S. Inflammation and metabolic disorders. *Nature* **444**, 860–867 (2006).
7. Wen, J. *et al.* Genetic, clinical underpinnings of subtle early brain change along Alzheimer’s dimensions. 2022.09.16.508329 Preprint at <https://doi.org/10.1101/2022.09.16.508329> (2022).
8. Liu, Y. *et al.* Genetic architecture of 11 organ traits derived from abdominal MRI using deep learning. *eLife* **10**, e65554 (2021).
9. Priest, C. & Tontonoz, P. Inter-organ cross-talk in metabolic syndrome. *Nat Metab* **1**, 1177–1188 (2019).
10. Jung, J., Zeng, H. & Horng, T. Metabolism as a guiding force for immunity. *Nat Cell Biol* **21**, 85–93 (2019).
11. McCracken, C. *et al.* Multi-organ imaging demonstrates the heart-brain-liver axis in UK Biobank participants. *Nat Commun* **13**, 7839 (2022).

12. Parlakg l, G. *et al.* Regulation of liver subcellular architecture controls metabolic homeostasis. *Nature* **603**, 736–742 (2022).
13. Nie, C. *et al.* Distinct biological ages of organs and systems identified from a multi-omics study. *Cell Reports* **38**, 110459 (2022).
14. Wen, J. *et al.* The Genetic Heterogeneity of Multimodal Human Brain Age. 2023.04.13.536818 Preprint at <https://doi.org/10.1101/2023.04.13.536818> (2023).
15. Bycroft, C. *et al.* The UK Biobank resource with deep phenotyping and genomic data. *Nature* **562**, 203–209 (2018).
16. Sanderson, E. *et al.* Mendelian randomization. *Nat Rev Methods Primers* **2**, 1–21 (2022).
17. Buniello, A. *et al.* The NHGRI-EBI GWAS Catalog of published genome-wide association studies, targeted arrays and summary statistics 2019. *Nucleic Acids Res* **47**, D1005–D1012 (2019).
18. Giambartolomei, C. *et al.* Bayesian Test for Colocalisation between Pairs of Genetic Association Studies Using Summary Statistics. *PLOS Genetics* **10**, e1004383 (2014).
19. Mummery, C. J. *et al.* Tau-targeting antisense oligonucleotide MAPTRx in mild Alzheimer’s disease: a phase 1b, randomized, placebo-controlled trial. *Nat Med* 1–11 (2023) doi:10.1038/s41591-023-02326-3.
20. Leeuw, C. A. de, Mooij, J. M., Heskes, T. & Posthuma, D. MAGMA: Generalized Gene-Set Analysis of GWAS Data. *PLOS Computational Biology* **11**, e1004219 (2015).
21. Nikolsky, Y. *et al.* Genome-wide functional synergy between amplified and mutated genes in human breast cancer. *Cancer Res* **68**, 9532–9540 (2008).
22. Wang, T. *et al.* Genome-wide DNA methylation analysis of pulmonary function in middle and old-aged Chinese monozygotic twins. *Respir Res* **22**, 300 (2021).

23. The Genotype-Tissue Expression (GTEx) project. *Nat Genet* **45**, 580–585 (2013).
24. Sakaue, S. & Okada, Y. GREP: genome for REPositioning drugs. *Bioinformatics* **35**, 3821–3823 (2019).
25. Wishart, D. S. *et al.* DrugBank 5.0: a major update to the DrugBank database for 2018. *Nucleic Acids Res* **46**, D1074–D1082 (2018).
26. Mittermayer, F. *et al.* Addressing Unmet Medical Needs in Type 2 Diabetes: A Narrative Review of Drugs under Development. *Curr Diabetes Rev* **11**, 17–31 (2015).
27. Finucane, H. K. *et al.* Partitioning heritability by functional annotation using genome-wide association summary statistics. *Nat Genet* **47**, 1228–1235 (2015).
28. Cahoy, J. D. *et al.* A Transcriptome Database for Astrocytes, Neurons, and Oligodendrocytes: A New Resource for Understanding Brain Development and Function. *J. Neurosci.* **28**, 264–278 (2008).
29. Bernstein, B. E. *et al.* The NIH Roadmap Epigenomics Mapping Consortium. *Nat Biotechnol* **28**, 1045–1048 (2010).
30. Dunham, I. *et al.* An integrated encyclopedia of DNA elements in the human genome. *Nature* **489**, 57–74 (2012).
31. Hwang, G. *et al.* Assessment of Neuroanatomical Endophenotypes of Autism Spectrum Disorder and Association With Characteristics of Individuals With Schizophrenia and the General Population. *JAMA Psychiatry* (2023) doi:10.1001/jamapsychiatry.2023.0409.
32. Wen, J. *et al.* Characterizing Heterogeneity in Neuroimaging, Cognition, Clinical Symptoms, and Genetics Among Patients With Late-Life Depression. *JAMA Psychiatry* (2022) doi:10.1001/jamapsychiatry.2022.0020.

33. Yang, Z. *et al.* A deep learning framework identifies dimensional representations of Alzheimer's Disease from brain structure. *Nat Commun* **12**, 7065 (2021).
34. Chand, G. B. *et al.* Schizophrenia Imaging Signatures and Their Associations With Cognition, Psychopathology, and Genetics in the General Population. *Am J Psychiatry* **179**, 650–660 (2022).
35. Ning, K. *et al.* Improving brain age estimates with deep learning leads to identification of novel genetic factors associated with brain aging. *Neurobiology of Aging* **105**, 199–204 (2021).
36. Jonsson, B. A. *et al.* Brain age prediction using deep learning uncovers associated sequence variants. *Nat Commun* **10**, 5409 (2019).
37. Smith, S. M. *et al.* Brain aging comprises many modes of structural and functional change with distinct genetic and biophysical associations. *eLife* **9**, e52677.
38. London, A., Benhar, I. & Schwartz, M. The retina as a window to the brain—from eye research to CNS disorders. *Nat Rev Neurol* **9**, 44–53 (2013).
39. Zhao, B. *et al.* Heart-brain connections: Phenotypic and genetic insights from magnetic resonance images. *Science* **380**, abn6598 (2023).
40. Zatorre, R. J., Fields, R. D. & Johansen-Berg, H. Plasticity in gray and white: neuroimaging changes in brain structure during learning. *Nat Neurosci* **15**, 528–536 (2012).
41. Tooley, U. A., Bassett, D. S. & Mackey, A. P. Environmental influences on the pace of brain development. *Nat Rev Neurosci* **22**, 372–384 (2021).
42. Zhao, B. *et al.* Common variants contribute to intrinsic human brain functional networks. *Nat Genet* **54**, 508–517 (2022).

43. Díaz Del Moral, S., Benaouicha, M., Muñoz-Chápuli, R. & Carmona, R. The Insulin-like Growth Factor Signalling Pathway in Cardiac Development and Regeneration. *Int J Mol Sci* **23**, 234 (2021).
44. Shen, H. *et al.* Mononuclear diploid cardiomyocytes support neonatal mouse heart regeneration in response to paracrine IGF2 signaling. *Elife* **9**, e53071 (2020).
45. Xu, Q. *et al.* The flavonoid procyanidin C1 has senotherapeutic activity and increases lifespan in mice. *Nat Metab* **3**, 1706–1726 (2021).
46. Tan, P., Jin, L., Qin, X. & He, B. Natural flavonoids: Potential therapeutic strategies for non-alcoholic fatty liver disease. *Front Pharmacol* **13**, 1005312 (2022).
47. Zhao, B. *et al.* Common genetic variation influencing human white matter microstructure. *Science* **372**, (2021).
48. Litviňuková, M. *et al.* Cells of the adult human heart. *Nature* **588**, 466–472 (2020).
49. Ballard, C. *et al.* Drug repositioning and repurposing for Alzheimer disease. *Nat Rev Neurol* **16**, 661–673 (2020).
50. Bulik-Sullivan, B. *et al.* An atlas of genetic correlations across human diseases and traits. *Nat Genet* **47**, 1236–1241 (2015).
51. Okun, J. G. *et al.* Liver alanine catabolism promotes skeletal muscle atrophy and hyperglycaemia in type 2 diabetes. *Nat Metab* **3**, 394–409 (2021).
52. Barsh, G. S., Farooqi, I. S. & O’Rahilly, S. Genetics of body-weight regulation. *Nature* **404**, 644–651 (2000).
53. Anandacoomarasamy, A., Caterson, I., Sambrook, P., Fransen, M. & March, L. The impact of obesity on the musculoskeletal system. *Int J Obes* **32**, 211–222 (2008).

54. Van Gaal, L. F., Mertens, I. L. & De Block, C. E. Mechanisms linking obesity with cardiovascular disease. *Nature* **444**, 875–880 (2006).
55. Stanikova, D. *et al.* Testosterone imbalance may link depression and increased body weight in premenopausal women. *Transl Psychiatry* **9**, 1–12 (2019).
56. Fyfe, I. Influence of amyloid- β on tau spread in Alzheimer disease explained. *Nat Rev Neurol* **18**, 318–318 (2022).
57. Barisano, G. *et al.* Blood–brain barrier link to human cognitive impairment and Alzheimer’s disease. *Nat Cardiovasc Res* **1**, 108–115 (2022).
58. Wyss-Coray, T. Inflammation in Alzheimer disease: driving force, bystander or beneficial response? *Nat Med* **12**, 1005–1015 (2006).
59. Wen, J. *et al.* Novel genomic loci and pathways influence patterns of structural covariance in the human brain. 2022.07.20.22277727 Preprint at <https://doi.org/10.1101/2022.07.20.22277727> (2022).
60. Purcell, S. *et al.* PLINK: A Tool Set for Whole-Genome Association and Population-Based Linkage Analyses. *Am J Hum Genet* **81**, 559–575 (2007).
61. Yang, J., Lee, S. H., Goddard, M. E. & Visscher, P. M. GCTA: A Tool for Genome-wide Complex Trait Analysis. *Am J Hum Genet* **88**, 76–82 (2011).
62. Watanabe, K., Taskesen, E., van Bochoven, A. & Posthuma, D. Functional mapping and annotation of genetic associations with FUMA. *Nat Commun* **8**, 1826 (2017).
63. Subramanian, A. *et al.* Gene set enrichment analysis: A knowledge-based approach for interpreting genome-wide expression profiles. *Proceedings of the National Academy of Sciences* **102**, 15545–15550 (2005).

64. Bulik-Sullivan, B. K. *et al.* LD Score regression distinguishes confounding from polygenicity in genome-wide association studies. *Nat Genet* **47**, 291–295 (2015).
65. Hemani, G. *et al.* The MR-Base platform supports systematic causal inference across the human phenome. *eLife* **7**, e34408 (2018).
66. Bowden, J. *et al.* A framework for the investigation of pleiotropy in two-sample summary data Mendelian randomization. *Stat Med* **36**, 1783–1802 (2017).
67. Bowden, J., Davey Smith, G. & Burgess, S. Mendelian randomization with invalid instruments: effect estimation and bias detection through Egger regression. *Int J Epidemiol* **44**, 512–525 (2015).

Acknowledgments

We want to express our sincere gratitude to the UK Biobank team for their invaluable contribution to advancing clinical research in our field. This study used the UK Biobank resource under Application Numbers: 35148 and 60698. Furthermore, we acknowledge the collaborative effort between the University of Southern California, the University of Pennsylvania, and the University of Melbourne in conducting this research. We gratefully acknowledge the support of the iSTAGING consortium, funded by the National Institute on Aging through grant R01 AG054409 at the University of Pennsylvania (CD). We also acknowledge the funding provided by the National Institute of Biomedical Imaging and Bioengineering at the University of Southern California through grant 5P41EB015922-25 (AT). Additionally, we acknowledge the funding program from the Rebecca L. Cooper Foundation at the University of Melbourne (AZ). Lastly, WJ would like to thank Paraskevi Parmpi and Jessica Incmikoski for their valuable administrative support during his postdoctoral research at AIBIL.